ON THE USE OF MARKOV RANDOM FIELD IN GEOPHYSICAL APPLICATIONS: GELIBOLU PENINSULA

JEOFİZİK UYGULAMALARDA MARKOV RANDOM FİLTRESİNİN KULLANIMI: GELİBOLU YARIMADASI

Osman N. UCAN[1] A. Muhittin ALBORA[2] and Davut AYDOĞAN[2]

[1)] Istanbul University, Engineering Faculty, Electrical & Electronics Department, 34850, Avcilar, Istanbul, Turkey

[2)] Istanbul University, Engineering Faculty, Geophysies Department, 34850, Avcilar, Istanbul, Turkey

ABSTRACT: : In this paper, Markov Random Field (MRF) approach is applied to gravity and magnetic anomaly map of Gelibolu Peninsula (Western Turkey) and complex fault structure of this region is modeled. We present a dynamic programming, MRF based on evaluation of noisy and super positioned effects of the various geological structures considering a statistical Maximum A Posteriori (MAP) criterion. We evaluate each pixel of N_1 xN_2 matrix using MRF approach, regarding the neighboring pixels and locality of their connections in real time with no priori processing. As synthetic examples, separation/ enhancement and edge detection performance of MRF is tested by various prism structures. After satisfactory results are found compared to classical derivative based approaches, as a real data, we have evaluated potential anomaly maps of Gelibolu Peninsula in the western region of Turkey.

Key Words: Markov Random Field (MRF), boundary determined, inverse solution, Gelibolu Peninsula

ÖZ: Bu makalede Markov Random Field (MRF) yaklaşımı Gelibolu yarımadasının gravite ve magnetic anomalisine uygulanmış, karmaşık fay system modellenmiştir. Maksimum olabilirlik yaklaşımına uygun olan istatitik bir dinamik program olan MRF ile farklı yeraltı cisimlerinin gürültülü ve üstüste bindirilmiş halleri incelenmiştir. MRF, ön eğitim gerektirmeyen, komşuluk ilişkisine dayalı reel zamanlı bir yaklaşımdır Sentetik olarak farklı prizmaların oluşturduğu anomalilerin kenar ve ayrışımı gerçekleştirilmiştir. Klasik modellere gore üstünlüğü belirlendikten sonar, Gelibolu bölgesi anomalisi değerlendirilmiştir.

Anahtar Kelimeler: Markov Random Filtre (MRF), Sınır saptama, ters çözüm, Gelibolu Yarımadası

INTRODUCTION

The application of update image processing techniques to geophysics result very successful evaluations. Satisfactorily separated Bouguer and magnetic anomalies help us to improve underground modeling of geological bodies. One of the main purposes of geophysical mapping is the identification of units that can be related to the unknown geology. On a regional scale, aeromagnetic and gravity maps are most useful tools presently available, although other techniques such as conductivity mapping Palacky (1986) or remote sensing Watson (1985) are very helpful in locating boundaries. These initial filtering operations include least squares minimization Abdelrahman, Bayoumi and El-Araby (1991), the Fast Fourier Transform methods Bhattacharryya and Navolio (1976) and recursive filters Vaclac, Jan and Karel (1992) and rational approximation techniques Agarwal and Lal (1971). Most of the works is concerned with gravity data, but many of the methods can be extended to magnetic data processing. Pawlowski and Hansen (1990) have investigated a potential anomaly separation method based on frequency-domain Wiener filtering. Shu-Kun, Jean-Claude and Chuen-TIen (1996) has presented a method for geological boundaries from potential-field anomalies. Albora *et al.* (2001a, b) have applied Cellular Neural Network (CNN) to gravity and magnetic anomalies and evaluated performance of CNN for real data.

The stochastic models depending on Markov Random Field (MRF) approach in 2-D data analysis has led to the development of many practical algorithms Derin and EllIot (1987), Geman and Geman (1984) that would not have been realized with *ad-hoc* processing. The literature of 2-D data analysis has experienced resurgence in the use of stochastic models to represent image data and to express prior, generic knowledge. The objective of MRF modeling is to capture the intrinsic character of data in a few parameters so as to unders-

tand the nature of phenomenon generating the data. The various applications of MRF are mainly achieved by Geman and Geman (1984), Derin and Elliot (1987), Dubes and Jain (1989), Ucan *et al*. (2000).

In this study, MRF has been applied to synthetic and real potential field data. In the proposed model, neighboring pixels and locality of their connections of the potential anomaly map are evaluated without priori information and no training. The new method is tested using synthetic examples and satisfactory results have been found. We have evaluated anomaly map of Gelibolu region and borders of the related faults are detected. The aim of this study is to enlighten the complex tectonic structure of Gelibolu peninsula using MRF approach. We have also modeled Anafartalar inverse fault and dike affecting the gravity and vertical magnetic anomaly maps obtained by Turkish Petroleum Anonymous Organization (TPAO). The tectonic structure of Gelibolu peninsula has been studied by many scientists. Elmas and Meric (1998) have defined another inverse fault on the North-West of Anafartalar fault. Yaltırak *et al*. (1998) have found a perpendicular directed fault on the same region. Ucan et al. (2001) have studied on gravity and magnetic anomalies of Saros Bay on the North-West of Gelibolu peninsula using wavelet approach. In this paper, we modeled tectonic structure of Gelibolu peninsula using MRF approach. We have also compared the results of inverse solutions with deep seismic cross-sections of TPAO and satisfactory results are found.

MARKOV RANDOM FIELD APPROACH

The magnetic anomaly of geological regions generally has low signal to noise ratio and there is background clutter and noise related with the different characterized geological structures. The classical approaches use local pixel intensity information to identify whether a pixel location is part of a boundary. Filters are used to collect local gradient information and, if the magnitude of the local gradient is large enough, the pixel is declared an edge pixel. Unfortunately, such techniques are sensitive to noise and, in addition, global boundary information is not available, which hinders the determination of closed objects boundaries.

The stochastic models depending on MRF approach in 2-D data analysis has led to the development of many practical algorithms (Dubes and Jain *et al.*, (1989); Geman and Geman (1984); Derin and Elliot (1987) that would not have been realized with ad-hoc processing. A random field is a joint distribution imposed on a set of random variables representing objects of interest, such as pixel intensities, that imposes the statistical dependence in a spatially meaningful way.

The objective of modeling is to capture the intrinsic character of data in a few parameters so as to understand the nature of phenomenon generating the data. The literature of 2-D data analysis has been experienced a resurgence in the use of stochastic models to represent image data and to express prior, generic knowledge. Given a realization of a Gibbs Random Field (GRF) and a defined model, we examine procedures for estimating the parameters in this GRF. Since only one realization is available and a complicated partition function is involved, the traditional statistical estimation methods are infeasible.

Potential anomaly map, we investigate is assumed to be a finite $N_1 \; X \; N_2$ rectangular lattice of points (pixels) defined as $L = \{(i, j) : \leq i \geq N_1, \; 1 \leq j \leq N_2\}$. A collection of subsets of L described as,

$$\eta = \{\eta_{ij} : (i, j) \in L, \eta_{ij} \subseteq L\} \qquad (1)$$

is a neighborhood system on if and only if the neighborhood of pixel (i, j). Hierarchically ordered sequences of neighborhood systems that are commonly used in modeling are η^1, η^2,..., $\eta^l = \{\eta^l_{ij}\}$ consisting of the closest four neighbors of each pixel known as nearest-neighbor model (Derin and Elliot, 1987). The usual neighborhood system in image analysis defines the first-order neighbors are the four pixels sharing a side within the given pixel. The neighborhood structures are given in Fig. 1. The neighborhood system is called the mth order neighborhood system. The neighborhood systems that can be defined over L are not limited to the hierarchical ordered sequence of the neighborhood system. A random field $X = \{X_{ij}\}$ defined on L has *Gibbs Distribution* or equivalently is a *GRF* with to η if and only if its joint

$$P(X = x) = \frac{(1)}{Z} e^{-U(x)} \qquad (2)$$

Figure 1. Hierarchically arranged neighborhood system η^m.
Şekil 1. η^m'in Hiyerarşik düzeltilmiş komşuluk sistemi.

distribution is of form,

$$U(x) = \sum_{c \in C} V_C(x),$$

where
defined as *energy function* and is potential function.

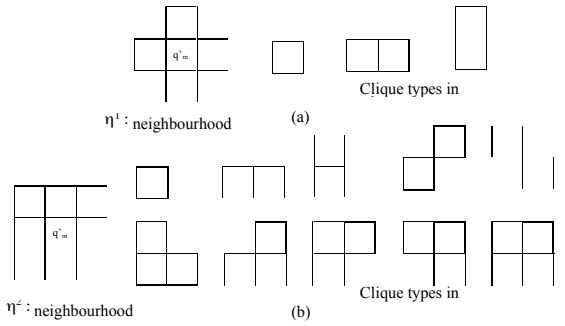

Figure 2. Neighborhood systems η^1 and η^2 their associated clique types.
Şekil 2. η^1 ve η^2 komşuluk sistemlerinde birbirleriyle komşuluk ilişkisi.

$V_c(x)$ is neighborhood type as in Figure 2. Defining the global energy functions is a powerful tool for specifying nonlinear interactions between different image features. They help to combine and organize spatial and temporal information by introducing strong generic knowledge

$$Z = \sum e^{-U(x)} \tag{3}$$

about the features to be estimated.

The joint distribution expression in (2) has the physical interpretation that the smaller energy function $U(x)$, the energy of the realization x, is the more likely that realization is [i.e., larger $P(X=x)$]. Minimizing the global energy function U is however usually a hard optimization problem: the number of possible label configurations is generally very large and moreover, the global energy function U may contain local minimal.

MRF is a very natural model that is able to translate local information and assumptions into a global model. In this paper, we describe a magnetic anomaly map $y=\{y_{ij}\}$ as an $N_1 \times N_2$ matrix of observations. It is assumed that this matrix y is a realization from a random field $Y=\{Y_{ij}\}$ which is the sum of magnetic fields produced by all underground sources. In our case, the targets for specific surveys are often small-scale structures buried at shallow depths, and the scene including these targets is defined as a residual random field $X=\{X_{ij}\}$. Contextual information enters through MRF model is its statistical dependence among the neighboring pixels. The random field X is a discrete valued random field, where X_{ij} takes values M quantization level as defined $Q = \{q_1, q_2, q_3, \ldots q_M\}$.

Correct estimation and removal of the regional field from initial field observations yields the residual field produced by the target sources. Interpretation and numerical modeling are carried out on the residual field data, and the reliability of the interpretation depends to a great extent upon the success of the regional-residual separation. In other words, given a magnetic anomaly map realization y, it is desired to determine residual scene x that given rise to y. The scene realization of x, of course, is not observed and can not be obtained deterministically from y. So the problem is to obtain an estimate $x^* = X^*(y)$ of the scene X, based on a realization y. Having set up the problem statistically, maximum *a posterior* estimation is chosen as statistical criterion (Derin and Elliot, 1987). So the objective now is to have an estimation rule, that is, an algorithm, which will yield x^* that maximizes the a posterior distribution $P(X = x/Y = y)$ for a given y. Applying Bayes rule, the a posterior

V_1	U_2	V_2
U_1	q'_m	U_3
V_3	U_4	V_4

Figure 3. q_m' and η_{ij} of residual magnetic map.
Şekil 3. q_m' *ve* η_{ij}*'nin manyetik anomali haritası.*

distribution can be written as (Fig. 2 and Fig 3.),

To maximize Eq. (5) for potential anomaly maps, we proposed MRF approach since in potential anomalies at the boundaries of regions of the original data, residual information is carried. It is also clear that traditionally, magnetic and magnetic maps are subjected to operations approximating certain functions such as second derivative and downward continuation. Then the two components of the joint log-likelihood in Eq. (5)

$$\ln P(X = x) = -\ln Z - \sum_{c \in C} V_C(x) \tag{6}$$

$$\ln P(Y = y/X = x) = -\frac{N_1 N_2}{2} \ln (2\pi\sigma^2) -$$

$$\sum_{m=1}^{M} \sum_{(i,j) \in S_m} \frac{1}{2\sigma^2} (s_{ij} - q_m)^2 \tag{7}$$

can be expressed for MRF as,
where $S_m = \{(i,j) \in L : X_{ij} = m\}$. σ is variance of the ima-

ge. Z is defined at Eq. (3), $q_m' \in q_m$ is the transient quantization level of residual map during optimization and $V_c\ (x)$ is the potential function. The joint log-likelihood ln *P(X=x,Y=y) Eq*. (5) is the sum of Eq. (6) and Eq. (7) and is to be optimized. Further information on this optimization procedure is given in Appendix A.

SYNTHETIC APPLICATIONS

The residual and regional separation/enhancement of potential anomalies is vital in geophysics. Edge detection of geological bodies can also be detected using various image processing techniques. The most interesting property of MRF is its high capacity of edge detection of buried structures as a result of separation in residual/regional anomalies. In MRF, using Equations (5-7) both neighborhood of pixels and general input image characteristics are taken into account. The decrement and increment of quantization levels show regional and residual effects respectively. In this synthetic example, three prisms are chosen with different depth, coordinates, inclination, declination angles and susceptibility values as given in Table I (Albora *et al*. 2001b). Here; X_1, X_2 and Y_1, Y_2 show the starting and ending coordinates of prisms at X and Y axes from the origin respectively. The shallow corner of the buried prisms are labeled as h_1, and deeper corner as h_2, inclination angle as I, declination angle as D, the angle between magnetic dipole and the prism as β and susceptibility as k. Total vertical magnetic anomaly of the prisms is shown in Fig. 4a.

Table 1. Magnetic Data Model with 3 prisms. Earth field (F)= 46000 nT, Inclination (I)= 67, Declination (D)= 25.
Tablo 1. 3 prizmanın oluşturduğu manyetik model Yerbileşen alanı (F)= 46000 nT (I)= 67, Denklinasyon (D)=25.

Prism	**XI**	**X2**	**Y1**	**Y2**	**h**	**H**	**I**	**D**	**β**	**χ**
Num.	Coor.	Coor.	Coor.	Coor.	Top of Depth	Bottom of Depth.	Inc.	Denc.	Prism Strike	Susc.
1	20	25	30	35	5	8	67	20	0	0.00193
2	32	36	17	21	4	6	66	24	5	0.00198
3	22	32	22	26	8	13	65	25	4	0.00205

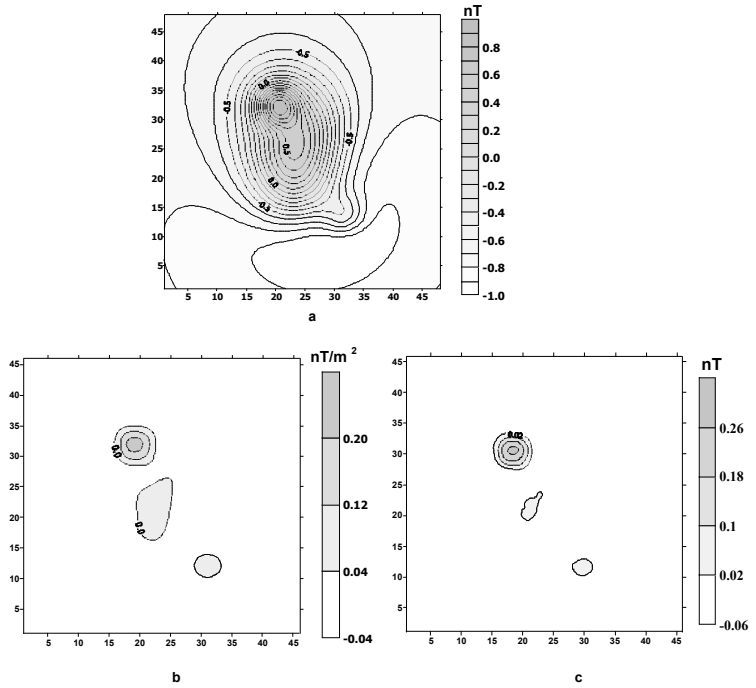

Figure 4. Evaluation of data obtained from Table I **a)** Total magnetic anomaly map (contour interval is 0.05 nT). **b)** Second vertical derivative of total magnetic anomaly map (contour interval is 0.08 nT/m²). c) MRF output (contour interval is 0.08 nT)

Şekil 4. Tablo I'den elde edilen dataların **a)** Toplam manyetik anomali haritası(kontur aralığı 0.05 nT).**b)** Toplam manyetik anomali haritasının ikinci düşey türevi çıktısı (kontur aralığı 0.08 nT/m²). c) MRF çıktısı (kontur aralığı 0.08nT)

To compare MRF with classical methods, second vertical derivative method is applied as in Fig. 4b. In MRF approach, average parameter vector θ defined in Eq. A6 is found as,

$$\theta = [\,0.0015, 0.0029, 0.0047, 0.0055, 0, 0.0067, \; -0.0213, 0, 0.0571, 0.0609, 0.0707, 0.0554]^T \quad (8)$$

Optimum quantization level is 8 and the residual anomaly map obtained at MRF output is given in Fig. 4c. The similar results are obtained in Fig. 4b and c. Thus we conclude that separation of potential anomalies using MRF is possible as in (Ucan *et al*. 2000).

As an another example, the vertical magnetic anomaly of two prisms perpendicular to each other are chosen in Fig. 5a to show the edge detection performance of MRF. We evaluate the same input data by using second vertical derivation as in Fig. 5b. In MRF approach, average parameter vector defined in Eq. A6 is found as,

$$\theta = [\,0.0314, 0, 0.0225, 0, 0.0219, -0.0061, -0.0561, -0.0137, 0.1350, 0.2394, 0.0747, 0.1272]^T \quad (9)$$

Optimum quantization level is 8 and the residual anomaly map obtained at MRF output is given in Fig. 5c. The similar results are obtained in Fig. 5b and c. After evaluation of these synthetic examples, we conclude that satisfactory results can be obtained for edge detection and separation/enhancement of geological bodies using MRF.

APPLICATION OF MRF TO REAL DATA: GELIBOLU PENINSULA

After satisfactory results are found in synthetic examples compared to classical derivative based approaches, as a real data, we have evaluated potential anomaly maps of Gelibolu Peninsula in the Western region of Turkey. As real data, we study on Gelibolu region of Turkey and find out fault map using MRF approach.

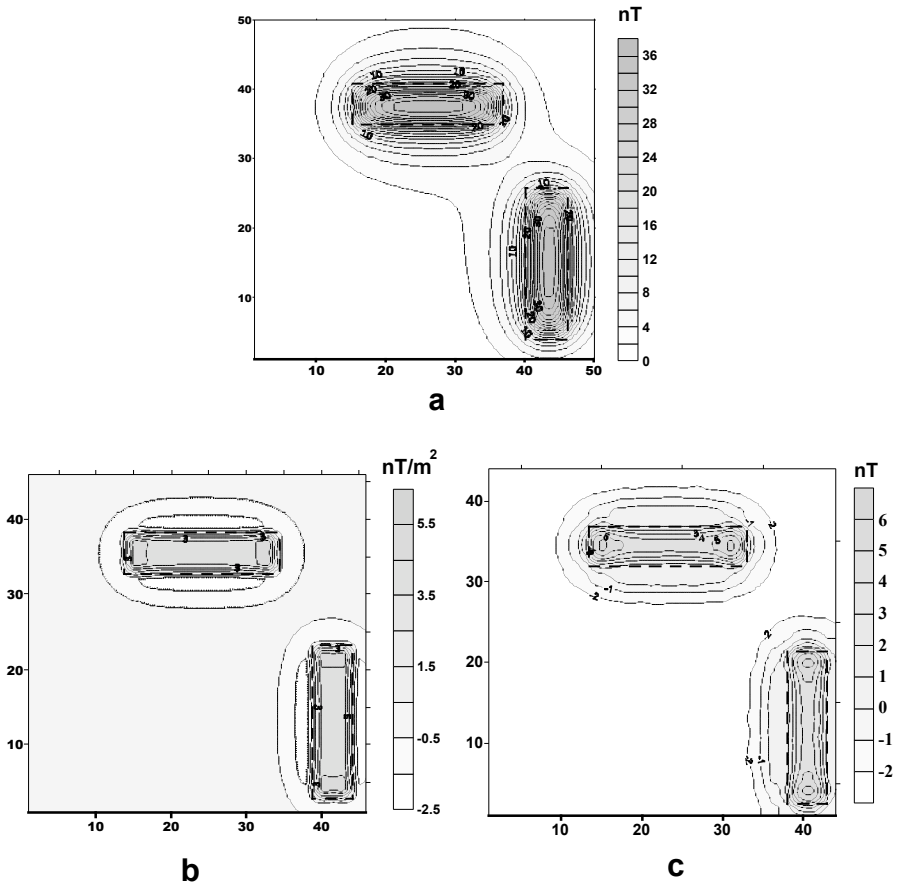

Figure 5. The synthetic model composed of two similar perpendicular prisms **a)** Vertical magnetic anomaly map (contour interval is 2 nT). **b)** Second vertical derivative of vertical magnetic anomaly map (contour interval is 1 nT/m^2). **c)** MRF output (contour interval is 1 nT).

Şekil 5. Birbirine dik olarak üretilen iki prizmanın **a)** Düşey manyetik anomaly haritası (kontur aralığı 2 nT). **b)** Düşey manyetik anomaly haritasının ikinci düşey türev çıktısı (kontur aralığı 1 nT/m^2). **c)** MRF çıktısı (kontur aralığı is 1 nT).

Cramplin and Evans 1986, Barka and Kadinsky-Cade 1988, have defined tectonic region with some fault branches having earthquake capacity, starting from the Marmara Sea and passes to North-East of Eagan Sea. Yaltırak *et al*. (1998) have found out the geological and tectonic structure of Gelibolu peninsula by their study in Saros Bay. Elmas and Meric (1998) have studied on the evaluation of tectonic of Marmara Sea and have given information on Gelibolu peninsula. Right lateral strike-slip fault which defines Southern margin of the Saros Graben and Anafartalar fault developed as positive flower structure in the late Miocene-Early Pliocene period. We have applied MRF filters for the gravity and magnetic anomalies obtained by TPAO.

Geology of Gelibolu Peninsula; In Gelibolu peninsula, there is cumulative sequence which is related to earlier ages as it starts from West to East of the region. The oldest part of the sequence is Upper Cretase which is Lower Paleosen aged Lort formation (Onal, 1986). On this sequence, there is Karaagac formation (Unal, 1967). At the upper layer, there is Fıcıtepe formation (Kellog, 1972; Yaltırak 1995). There are also Ceylan, Mezardere, Osmancık formations on Sogucak formation and top on them Gazhanedere formation takes place (Yaltırak 1995). Gazhanedere formation continues through out Anafartalar fault (Fig. 6). All these formations are shown in seismic cross-section in Figure 7.

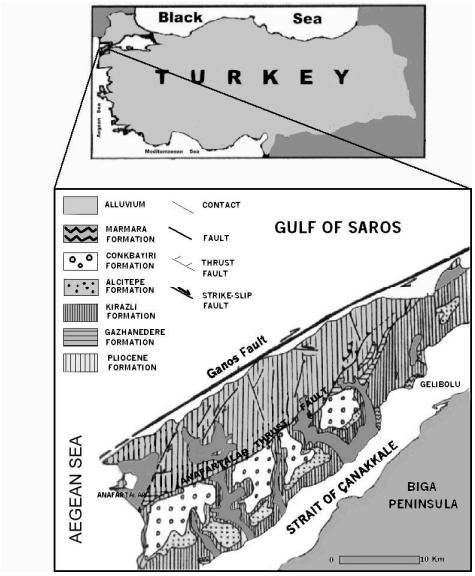

Figure 6. Geology of Gelibolu Peninsula (modified form of Yaltirak 1995 and Yaltırak et. al 1998).
Şekil 6. Gelibolu Yarımadasının Jeolosisi (Yaltirak 1995 and Yaltırak vd. 1998'den değiştirilerek alınmıştır).

Figure 7. Deep seismic cross-sections, DG-158 and DG-159 (obtained by TPAO).
Şekil 7. DG-158 ve DG-159 derin sismik kesit (TPAO tarafından alınmıştır).

Tectonic of Gelibolu Peninsula; There is an important fault, named as Anafartalar in this region at the Northeast direction with 45 degree. In deep seismic drilling outputs, DG-158 and DG-159 of TPAO, Anafartalar inverse fault is clearly observed. Ganos fault, which is the North part of North Anatolian Fault (KAF), places at the Northwest direction of Gelibolu peninsula (Ucan *et al.,* 2001). It is clear that Gelibolu peninsula has complex earth structure and thus has many faults.

INTERPRETATION OF GRAVITY AND MAGNETIC ANOMALY MAPS

In evaluation of magnetic anomaly map of Gelibolu peninsula (Fig. 8), at the middle regions 6400 nT

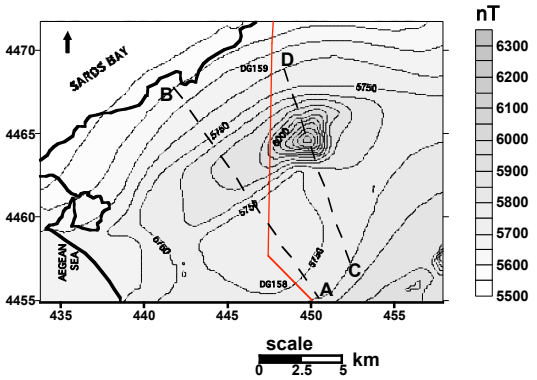

Figure 8. Magnetic anomaly of Gelibolu Peninsula (A-B and C-D profiles are shown in dashed lines, DG 158 and DG 159 seismic cross-sections are also shown in continuous lines).

Şekil 8. Gelibolu yarımadasının manyetik anomaly haritası (A-B ve C-D kesik çizgiler ile gösterilen profiler, DG 158 ve DG 159 düz çizgi ile gösterilen sismik kesit profili).

amplitude is observed. We believe that one of the main reason of this increment in amplitude is Ganos fault. The effect of Anafartalar fault and Ganos fault overlap each other, thus resulting amplitude increment and continues up to Saros Bay which lies on the West side of Gelibolu region (Ucan *et al.* 2001). This property is clearly seen at deep seismic cross-section DG-158 in Figure 7. C-D profile is shown in dashed lines in magnetic anomaly map in Figure 7. Inverse solution is proposed for dike model parameters. In inverse solution method, LIMAT software program is used which is developed by Venkataraju (2003). The magnetic profile C-D which is located at with a strike direction SE-NW, is taken 6000 m in length, sampled at 250 m interval. The process is terminated at the 38th iteration, since there is no significant change in the value of objective function. The depth to top of dike model is z=991.51 m, slope is θ=37.70°, the distance of the origin from the reference point R is d=3754.84 m, width of dike is b=40.84 m and susceptibility contrast is χ=0.1426 SI. The base slope is A=-0.02 nT/m and base level is found as C=5779.62 nT. The proposed dike model is obtained as in Figure 9 by inverse solution regarding measured anomaly values and parameters.

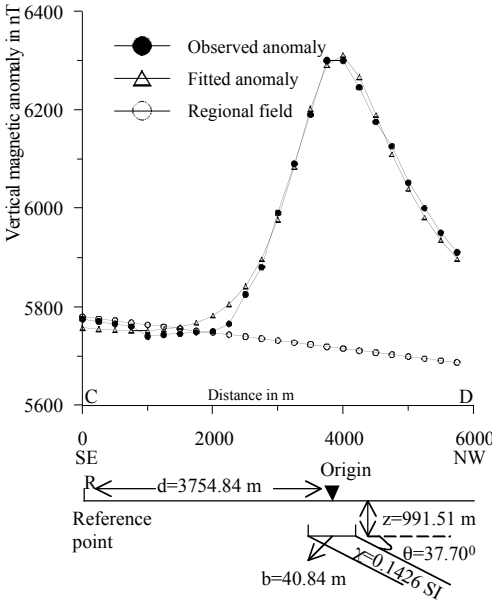

Figure 9. CD vertical magnetic anomaly and its interpretation

Şekil 9. CD düşey manyetik anomali haritasından alınan kesitin yorumu.

Markov Random Field approach is applied to vertical magnetic anomaly map shown in Figure 8 and average parameter vector θ defined in Eq. A6 is found as,

$$\theta = [0,-0.1504,0.0525,0.0447,0.0334,0.0118,0.0081,0,-0.0069,-0.0206,-0.0152,0.0084]^T \quad (10)$$

and optimum quantization level is 8 as in Figure 10. The tectonic structures obtained from the research results of Yaltırak et al. (1998), are also drawn in MRF output. In MRF, dike type geological structure is better shown. The Anafartalar inverse fault effect is well defined because of high edge detection performance of MRF. By using A-B profile of Figure 8, Anafartalar inverse fault is modeled. Tfaultin software program of Radhakrishna Murthy *et al.* (2001) is used in inverse modeling. The profile A-B which is located at with a strike direction SE-NW, is taken 7 km in length, sampled at 250 m interval. The process is terminated at the 50 iteration since there is no significant change in the value of objective function. The upper and lower depth of fault model is

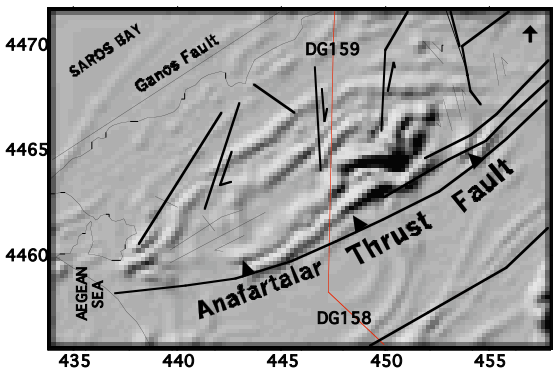

Figure 10. MRF output of Gelibolu Peninsula magnetic anomaly map given in Figure 8. (Tectonic lines are drawn obtained by Yaltırak et al,1998).

Şekil 10. Şekil 8'de verilen Gelibolu Yarımadası manyetik anomali haritasının MRF çıktısı (Tektonik çizgiler Yaltırak vd. 1998'den alınmıştır

z_1=1.06 km and z_2=3.77 km, respectively. The distance from the arbitrary initial coordinate to the end point of fault is 4.52 km, fault angle is θ=66.63° and susceptibility contrast is χ=0.002 SI. The base slope is A=13.04 nT/m and base level is found as C=5746 nT. The proposed fault model is obtained as in Figure 11 by inverse solution regarding measured anomaly values and parameters.

In the evaluation of gravity anomaly map, there observed an anomaly increment from South-East to North-West direction as in Figure 12. his increment starts with –6 mgal up to 40 mgal. One of the main reason of this increment is Ganos fault. Ganos fault effects starts before the Anafartalar fault effect minimizes and thus this overlapping results the anomaly amplitude increment and continues up to Saros Bay (Ucan *et al.* 2000).

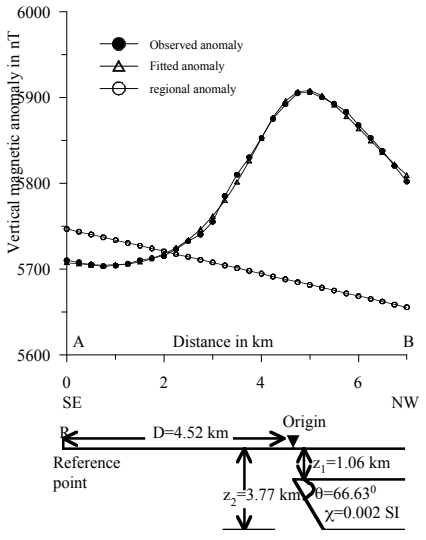

Figure 11. Geological structurel model regarding data obtained by A-B profile of magnetic anomaly in Figure 8.

Şekil 11. Şekil 8'de verilen manyetik anomali haritasında A-B profilinden hesaplanan jeolojik yapı modeli.

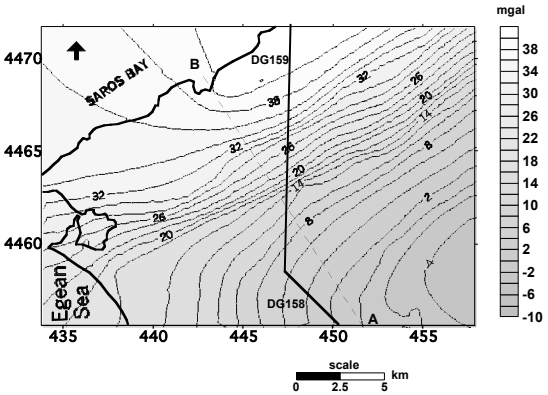

Figure 12. Bouguer anomaly map of Gelibolu Peninsula (A-B profile are shown in dashed lines).

Şekil 12. Gelibolu Yarımadasının Bouguer anomaly haritası (A-Bprofili kesik çizgiler ile gösterilmiştir).

We have applied MRF to the gravity anomaly map in Figure 12 and the results are shown in Figure 13.

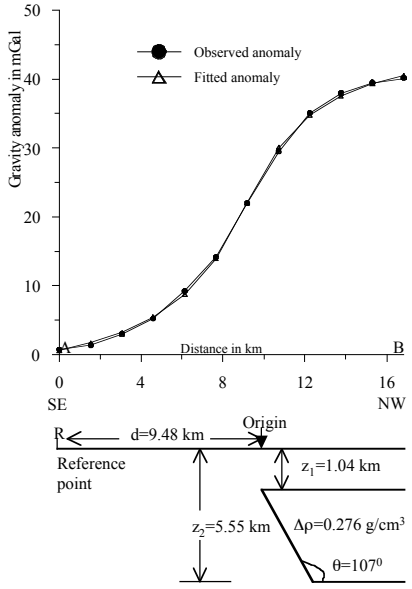

Figure 13. AB gravity anomaly profile and the derived structural model

Şekil 13. A-B gravite anomaly profilinden elde edilen yapısal model.

In MRF approach, average parameter vector defined in Eq. A6 is found as,

$$\theta = [-0.0438, 0.0153, 0, 0.0061, 0.0191, -0.0270, 0.0304, 0, -0.0155, 0.0047, 0.0179, 0.1521]^T \quad (11)$$

and optimum quantization level is 8. In Figure 13, the effect of Anafartalar inverse fault is clearly seen. We have modeled Anafartalar fault by cross-section of A-B shown by dashed line in Figure 12. We have used simulation program developed by Aydogan (1993), which is capable of modeling regarding to density distributions and parameters of geometric structures at any arbitrary initial coordinates. The profile AB which is located at with a strike direction SE-NW is taken 16.83 km in length from the gravity anomaly map. This profile is assumed as a fault, which can be interpreted by the truncated horizontal-plate model. The process is terminated at the 20th iteration since there is no significant change in the value of objective function. The upper and lower depth of fault model is z_1=1.04 km and z_2=5.55 km, respectively. Slope angle is θ=107° and the distance from the arbitrary initial coordinates to the end point of the fault is d=9.48 km and density contrast is $\Delta\rho$=0.276 g/cm^3. The results of inversion are shown in Figure 14.

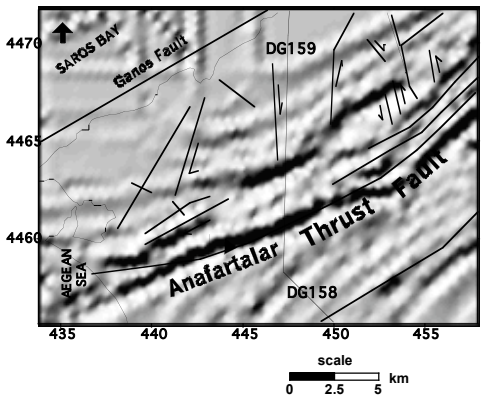

Figure 14. AB gravity anomaly profile and the derived structural model

Şekil 14. A-B gravite anomaly profilinden elde edilen yapısal model.

CONCLUSION

In this paper, we have applied Markov Random Field (MRF) for both synthetic examples and real geophysical data of Gelibolu region which lies in the European part of Turkey. We have obtained these Bouguer and vertical magnetic anomaly maps from TPAO. We have especially chosen this area, since it has complex structures with many faults overlapping each others. We achieved to detect the borders of various synthetic examples and also to separate residual/regional anomalies. We compared our results with classical second derivative method. Then we evaluated the fault characteristics of the real data. We proposed tectonic model of Gelibolu regarding to MRF output as in Figure 15. Especially the effect of the inverse fault is dominant. Ganos lateral fault lies on the North-West of Anafartalar and is important for its potential earthquake. In the studies of Yaltırak et al. (1998), Anafartalar fault is defined as one fault which can be seen from geological maps. Here, we have detected another parallel fault on the North-West of Anafartalar fault using MRF filtering techniques. These results are also supported by the study of Elmas and Meriç (1998). This property is also obtained in seismic cross-section. This overlapping can be

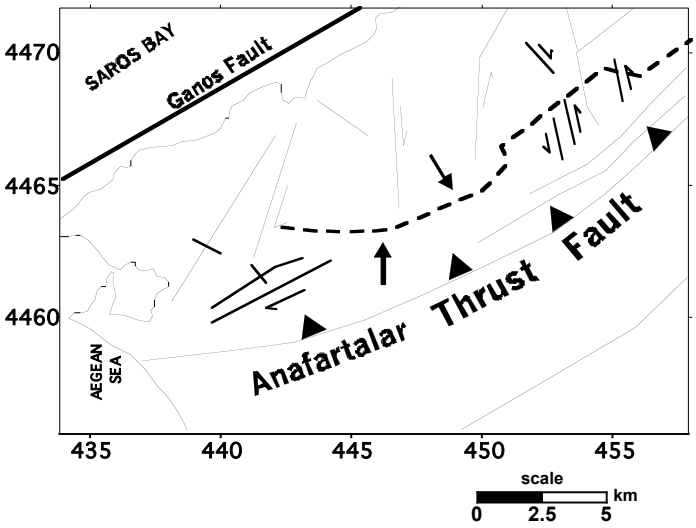

Figure 15. Tectonic map obtained by MRF output (The region shown in dashed lines and arrows are prepared due to MRF filtering).

Şekil 15. MRF çıktısı sonucunda elde edilenTektonik harita (Bölgede gösterilen kesik çizgiler MRF çıktısı sonucunda elde edilmiştir.

explained as Anafartalar fault goes deeper and older aged faults comes up closer to the surface, resulting an active fault structure. In MRF of gravity anomaly maps, the similar structure is also observed at the North-West of Anafartalar inverse fault.

We have drawn the results of Yaltırak *et al.* (1998) in MRF filtering of gravity and magnetic anomalies to compare our outputs with previous studies in this region. In geological map, our results are confirmed by previous geological studies for the South-East of Anafartalar inverse fault, but on the North-West of this fault, we have detected another parallel fault. Anafartalar fault goes deeper while the structure on North-West overlaps. We can say that this overlapping is occurred due to the Ganos fault on the North and has an important tectonic effect on this region (Ucan *et al.* 2001).

In Figures 10 and 13, MRF is applied to magnetic and gravity anomaly maps as in Figure 8 and 12, respectively. In evaluation of MRF outputs, we conclude that in Gelibolu region, there is Anafartalar fault, but there is also another parallel fault at the North-West of Anafartalar fault. This result is also confirmed by deep seismic studies in Figure 7. The effect of the lateral fault is also observed at coordinates near to 6400 nT values of magnetic anomaly map in Figure 8. The overlapping of the considered lateral fault with higher susceptibility and anomaly amplitude results this increment. This anomaly increment can also be explained as the difference between susceptibilities of C-D profile (Fig. 9) and A-B profile (Fig. 11) of dike models. We have also modeled tectonic structure of this region (Fig. 15). Thus we believe that MRF will be compromising filtering techniques in geophysics.

ÖZET

Bu makalede, Markov Random Filtre tekniği Gelibolu Yarımadasında (BatıTürkiye) elde edilen Gravite ve manyetik anomali haritalarına uygulanarak oldukça karmaşık bir yapıya sahip olan bölge modellenmiştir. MRF, eğitim gerektirmeyen önsel bilgiye ihtiyaç olmayan eşsiz bir algoritmadır. Program gürültülerin elemine edilmesinde olumlu neticeler vermektedir. MRF yönteminin en önemli özelliği, komşuluk ve iki boyutlu görüntünün stokastik özelliklerinden faydalanılması ve ön eğitim gerektirmemesidir. Bu makalede, gravite ve manyetik anomali haritaları N_1 x N_2 boyutlu görüntü olarak alınmıştır. Biz her bir pikseli N1*N2 matris olarak değerlendiririz. Bu görüntü yeraltındaki farklı yapıların etkileşiminden oluştuğu varsayılmıştır. MRF uygulaması ile rezidüel yapıların ortaya çıkarılması sağlanmış ve $x=\{x_{ij}\}$ şeklinde belirlenmiştir. MRF yöntemini test etmek amacıyla çeşitli prizmatik yapıların ayrım/ iyileştirme konusundaki başarısı ile kenarların saptanmasındaki başarısına bakılmıştır. Ayrıca Türkiye'nin batısındaki Gelibolu yarımadasının potansiyel potansiyel anomali haritalarının hesaplanmasında klasik türev yöntemleri ile karşılaştırma yapılmıştır MRF yöntemi kullanarak potansiyel kaynaklı haritaların çıktılarını aldık ve ters çözüm tekniği kullanarak jeolojik yapıları modelledik.Ters çözüm tekniği kullanarak elde edilen modeller ve MRF sonucunda elde edilen jeoljik yapıların sonuçlarıTPAO elde edilen derin sismik kesitler ile karşılaştırılmıştır Jeolojik yapıların sınırlarının saptanmasında ayrım/iyileştirme MRF yaklaşımının başarılı sonuçlar verdiğini söyleyebiliriz.

ACKNOWLEDGEMENT

We thank TPAO who have given the data of Gelibolu Penisula. This project is supported by Istanbul University, Research Fund. Project No:1539/16012001, 1409/0505200

REFERENCES

Abdelrahman, E. M., Bayoumi, A. I., and El-Araby, H. M., (1991), A least-squares minimization approach to invert gravity data, Geophysics. 56, 115-118.

Agarwal, B. N. P., and Lal, L. T., (1971), Application of rational approximation in the calculation of the second derivative of the gravity field, Geophysics. 36, 571-581.

Albora, A. M., Ucan, O. N., Ozmen, A., and Ozkan, T., (2001a), Separation of Bouguer anamoly map using cellular neural network, Journal of Applied Geophysical. 46, 129-142.

Albora, A. M., Ucan, O. N., and Ozmen, A., (2001b), Residual Separation of Magnetic Fields Using a Cellular Neural Network Approach, Pure and Applied Geophysics. 158, 1797-1818.

Aydogan, D., (1993), Computation of gravimetric model parameters by Monte Carlo Method, Turkish Geophysics. 7, 35-47.

Barka, A. A., and Kadinsky-Cade, K., (1988), Strike-slip fault geometry in Turkey and its influence on earthquake activity, Tectonics. 7, 3, 663-684.

Bhattacharryya, B. K., and Navolio, M. E., (1976), A Fast Fourier Transform method for rapid computati-

on of gravity and magnetic anomalies due to arbitrary bodies, Geophysics Prosp. 20, 633-649.

Cramplin, S., and Evans, R., (1986), Neotectonic of the Marmara Sea region in Turkey, Jour. Geol. Soc. Lond. 143, 343-348.

Derin, H., and Elliot, A. H., (1987), Modeling ans segmentation of noisy and textured images using Gibbs Random Field, IEEE PAMI. 9, 39-55.

Dubes, R. C., and Jain, A., (1989), Random field models in image analysis, Journal of Applied Statistics. 16, 131-162.

Elmas, A., and Meric, E., (1998), The Seaway Connection between the Sea of Marmara and the Mediterranean, Tectonic Development of the Dardanelles, International Geology Review. 40, 144-162.

Geman, S., and Geman, D., (1984), Stochastic Relaxation, Gibbs Distributions, and the Bayesian restration of images, IEEE PAMI. 6, 721-741.

Kellog, B. H., (1972), Geology and Petroleum Prospects Gulp of Saros and vicinity SW Trace, Ashland Oil of Turkey, TPAO Rapor No: 902.

Onal, M., (1986), Sedimentary sequences and Tectonics of central part of Gelibolu Penisula, Nortwest Anatolia, Turkey, I.U. Engineering Faculty's Earth Sciences Review. 5, 21-38.

Palacky, G. J., (1986), Geological background to resistivity mapping, in Airborne resistivity Mapping (Palacky, G. J., ed.) (G.S.C.) 86-22,19-27.

Pawlowski, R. S., and Hansen, R. O., (1990), Gravity anomaly separation by Wiener filtering, Geophysics. 55, 539-548.

Radhakrishna Murty, I. V., Swamy, K. V., and Jagannadha Rao, S., (2001), Automatic inversion of magnetic anomalies of faults, Computers & Geosciences. 27, 315-325.

Shu-Kun, H., Jean-Claude, S., and Chuen-Tien, S., (1996), High-resolution detection of geological boundaries from potential-field anomalies: An enhanced analytical signal technique, Geophysics. 61, 373-386.

Ucan, O. N., Şen, B., Albora, A. M., and Özmen, A., (2000), A New Gravity Anomaly Separation Approach: Differential Markov Random Field (DMRF), Electronic Geosciences. 5,1.

Ucan, O. N., Albora A. M. and Hisarlı, Z. M., (2001), Comments on the Gravity and Magnetic Anomalies of Saros Bay using Wavelet approach, Marine Geophysics. 22, 251-264.

Vaclac, B., Jan, H., and Karel, S., (1992), Linear filters for solving the direct problem of potential fields, Geophysics. 57, 1348-1351.

Venkata Raju, D. Ch., (2003), LIMAT: a computer program for least-squares inversion of magnetic anomalies over long tabular bodies, Computers & Geosciences. 29, 91-98.

Yaltırak, C., (1995), Tectonic Mechanism Controlling the Plio-Quaternary Sedimentation in the Gelibolu Peninsula, Turkish Geophysics (Nezihi Canitez Symposium). 9, 103-106.

Yaltırak, C., Alpar, B., and Yuce, H., (1998), Tectonic elements controlling the evolution of the Gulf of Saros (northeastern Aegean Sea, Turkey), Tectonophysics. 300, 227-248.

Watson, K., (1985), Remote sensing: A geophysical perspective, Geophysics. 55, 843-850.

APPENDIX A

Using similar optimization approach of Derin and Elliot (1987), we present the formulation in terms of a second order neighborhood system η^2, although its extension to any order is possible. Consider a site *(i,j)* and its neighborhood $\eta_{i,j}$ at residual map of *X*. Let q_m' is the transient quantisation level of residual map during optimization at *(i,j)* pixel and t' represent the vector of neighboring values of q_m' at *(i,j)*.

$$t' = [u_1, u_2, u_3, u_4, v_1, v_2, v_3, v_4] \tag{A1}$$

where the location of u_i's and v_i's with respect to q_m'. We define indicator functions,

$$I(z_1, z_2 \ldots, z_k) = \begin{cases} -1 & , z_1 \approx z_2 \\ 1 & , \text{otherwi} \end{cases} \tag{A2}$$

$\approx$ is the approximation defined as,

$$z_k \approx z_{k+1} \cong |z_k - z_{k+1}| \le \varepsilon \tag{A3}$$

where ε is a small value given regarding to optimization tolerance. Another indicator $J_m(q_m')$ is defined as,

$$J_m(q_m') = \begin{cases} -1 & , q_m' \approx q_m \\ 1 & , \text{otherw} \end{cases} \tag{A4}$$

Using these indicators we can express the potential function Eq. (7) of all cliques that contain *(i, j)*, the site of (Fig. 1). That is

$$V(q_m', t', \theta) \equiv \sum_{c:q_m'} V_C(x) \quad \text{(A5)}$$

where θ is the parameter vector. Thus both Eq. (6) and Eq. (7) are defined as a function of q_m', resulting common optimization which improves the MRF performance greatly. θ is defined as (Derin and Elliot (1987),

$$\theta = [\alpha_1, \alpha_2 .., \alpha_M, \beta_1, \beta_2, \beta_3, \beta_4, \gamma_1, \gamma_2, \gamma_3, \gamma_4, \xi_1]^T \quad \text{(A6)}$$

The clique potentials associated with are defined as,

$$\begin{bmatrix} * & * \\ & , \beta_1 \end{bmatrix}, \begin{bmatrix} * \\ * & , \beta_2 \end{bmatrix}, \begin{bmatrix} & * \\ * & , \beta_3 \end{bmatrix}, \begin{bmatrix} * \\ & *, \beta_4 \end{bmatrix}, \begin{bmatrix} * & * \\ * & \gamma_1 \end{bmatrix}, \begin{bmatrix} * \\ * & * \gamma_2 \end{bmatrix},$$
$$\begin{bmatrix} & * \\ * & * \gamma_3 \end{bmatrix}, \begin{bmatrix} * & * \\ * & * \xi_1 \end{bmatrix}. \quad \text{(A7)}$$

where, in $\begin{bmatrix} * & * \\ & , \beta_1 \end{bmatrix}$ expression, we are related with only right adjacent pixel (u_1) and left adjacent pixel (u_2) of our observed pixel (s) as shown in Fig. 1. The other expressions of Eq.s (A6-7) can easily evaluated in the same manner. We can rewrite Eq. (A5) as,

$$V(q_m', t', \theta) \equiv \phi^T(q_m', t')\,\theta. \quad \text{(A8)}$$

where,

$$\phi(q_m', t') = [J_1(q_m') + J_2(q_m'), ..., J_M(q_m'), (I(q_m', u_1 + I(q_m', u_3)), (I(q_m', u_2) + I(q_m', u_4)), (I(q_m', v_2) + I(q_m', v_4)), (I(q_m', v_1) + I(q_m', v_3)), (I(q_m', u_2, v_2) + I(q_m', u_4, u_3) + (I(q_m', u_1 v_4)), (I(q_m', u_4 v_3 + I(q_m', u_2, u_3) + (I(q_m', u_4 v_3) + I(q_m', u_2 u_3 + I(q_m', u_1, v_1)), (I(q_m', u_2 v_1) + I(q_m', u_1 u_4 + I(q_m', u_3, v_3)), (I(q_m', u_1 u_2) + I(q_m', u_4 v_4 + I(q_m', u_3, v_2)), (I(q_m', u_1 v_1 u_2) + I(q_m', u_2 v_2 u_3) + I(q_m', u_3, v_3, u_4) + I(q_m', u_4 v_4 u_1))]^T \quad \text{(A9)}$$

Suppose $P(q_m', t')$ is the joint distribution of random variables on 3*x*3 block centered at *(i, j)* and $P(t')$is the joint distributions on η_{ij} only. Then the conditional probability, using Bayes rule can be written as,

$$\frac{P(q_m', t')}{P(t')} = P(q_m'/t') = \frac{e^{-V(q_m', t', \theta)}}{W(t', \theta)} \quad \text{(A10)}$$

where

$$W(t', \theta) \equiv \sum_{s \in Q} e^{-V(q_m', t', \theta)} \quad \text{(A11)}$$

Rearranging,

$$\frac{e^{-V(q_m', t', \theta)}}{P(q_m', t')} = \frac{W(t', \theta)}{P(t')} \quad \text{(A12)}$$

is obtained. Considering only left hand side of Eq. (A12), for two distinct values of $q_m' = j$, $q_m' = k$ values we have,

$$e^{-V(j, t', \theta) + V(k, t', \theta)} = \frac{P(j, t')}{P(k, t')} \quad \text{(A13)}$$

Taking the natural logarithm of (A13) and replacing (A8), we obtain,

$$(\phi(k, t') - \phi(j, t'))^T\ \theta = \ln \frac{P(j, t')}{P(k, t')}) \quad \text{(A14)}$$

In (A14), the vector $(\phi(k,t') - \phi(j,t'))$ is determined easily for any *j, k, t'* while θ is the unknown parameter to be estimated. The question that remains to be replied is how to determine $P(q_m', t')$ values. We achieve these using histogram techniques. As a result, we have explained how to extract residual magnetic map using Markov Random Field approach.

Yayına Geliş - *Received* : 30.12.2003
Yayına Kabul - *Accepted* : 06.05.2004